Article

Synthesis of Silver and Gold Nanoparticles in Sodium Alginate Matrix Enriched with Graphene Oxide and Investigation of Properties of the Obtained Thin Films

Nikola Nowak [1], Wiktoria Grzebieniarz [1], Gohar Khachatryan [1,*], Karen Khachatryan [1], Anna Konieczna-Molenda [1], Marcel Krzan [2] and Jacek Grzyb [3]

1 Faculty of Food Technology, University of Agriculture in Krakow, Balicka Str. 122, 30-149 Krakow, Poland; nikola.nowak@urk.edu.pl (N.N.); wiktoria.grzebieniarz@urk.edu.pl (W.G.); karen.khachatryan@urk.edu.pl (K.K.); anna.konieczna-molenda@urk.edu.pl (A.K.-M.)
2 Jerzy Haber Institute of Catalysis and Surface Chemistry, Polish Academy of Sciences, 30-239 Krakow, Poland; marcel.krzan@ikifp.edu.pl
3 Faculty of Agriculture and Economics, University of Agriculture in Krakow, Mickiewicz Ave. 21, 31-120 Krakow, Poland; jacek.grzyb@urk.edu.pl
* Correspondence: gohar.khachatryan@urk.edu.pl

Abstract: Polymer nanocomposites containing nanometals became a subject of interest due to their bactericidal properties. Different polysaccharides have been used as matrices for nanosilver and nanogold synthesis. In this study, we present a novel, environmentally friendly method for the preparation of sodium alginate/nanosilver/graphene oxide (GOX) and sodium alginate/nanogold/graphene oxide GOX nanocomposites and their characteristics. The formation of approximately 10–20 nm ball-shaped Ag and Au nanoparticles was confirmed by UV–vis spectroscopy, scanning electron microscopy (SEM) and Fourier transform infrared (FTIR) spectra. The incorporation of GOX sheets within the ALG matrix improved the thermal stability of the nanocomposites film, which was measured using the differential scanning calorimetry (DSC). We also estimated the molecular weights of polysaccharide chains of the matrix with the size exclusion chromatography coupled with multiangle laser light scattering and refractometric detectors (HPSEC-MALLS-RI). The composites were more prone to enzymatic hydrolysis. The strongest bacteriostatic activity was observed for the sample containing nanosilver.

Keywords: polysaccharides; sodium alginate; nanocomposites; graphene oxide; nanosilver; nanogold

1. Introduction

Polysaccharides are a cheap, sustainable and renewable group of commonly available organic compounds. They are considered as attractive resources for obtaining several novel biodegradable materials, attractive for medicine, chemical and pharmaceutical industries or food technology. Natural polysaccharides are enjoying a growing interest for their spreading fields of potential applications [1].

For their chemical structure, polysaccharides can be readily modified by involving physical, physicochemical, chemical and enzymatic methods. Numerous studies confirm the bioactivity of polysaccharides, providing their applications in clinical practice, nutrition and dietetics [2]. Depending on their origin, polysaccharides exhibit antioxidative, immunomodulating, anti-inflammatory, antiviral (among others, HIV), antimutagenic, cancerostatic and anticlotting properties [3–5].

Sodium alginate is a linear polymer composed of D-mannuronic and L-guluronic acid blocks. It has been approved by the US Food and Drug Administration (FDA) for human use in certain biomedical applications [6]. As a polysaccharide hydrogel, it finds various applications in industry, for example, in biodegradable plastic packaging materials [7], medicine and biotechnology [8]. It is non-toxic, biodegradable, biocompatible and has a far lower cost than many other biopolymers. It is also renewable [9].

Recent studies recognized the applicability of various polysaccharides in the synthesis of inorganic nanoparticles [10–12]. Polysaccharides act as reducers and stabilizers—matrices, providing the formation of nanoparticles uniform in size and satisfying, in this manner, requirements for their practical applications [13]. Nanoparticles immobilized within such matrices exhibit all the demanded properties: functionality, barrier properties, transparency and other interesting features. Nanocomposites with such nanoparticles are biodegradable and environmentally benign. Thus, they enjoy numerous potential applications, such as in prophylaxis, therapy and agricultural production [14]. The most suitable polysaccharides in developing nanoparticles are: starch, cellulose, alginates, pectins, xanthan gum, cyclodextrins, chitosan [15], heparin [16], furcellaran [17] and hyaluronic acid [18–20].

The mechanical properties of the polysaccharide materials can be improved with some additives such as hydrophobic materials and plasticizers [21,22]. Inorganic compounds are alternative additives [23,24]. Some papers announce the use of graphene oxide for this purpose [25–27]. Graphene and its derivatives are monolayer carbon materials. Their unique bidimensional structure offers a large surface, adsorbing nucleic bases and aromatic compounds involving π–π interactions. Epoxy, hydroxyl and carboxylic groups facilitate their conjugation with biomolecules [28]. Erqun Song [29] has presented a novel nanohybrid of hyaluronic acid and graphene oxide for a device sensitive to pH changes of drug carriers. This hybrid successfully liberated cancerostatic doxorubicin. Recent studies have also investigated the antibacterial effect of graphene oxide occurring due to its interactions with bacterial cell membranes [30–32].

As with other nanoparticles, graphene exhibits a tendency to aggregation via the van der Waals interaction between graphene layers. This behavior limits graphene applications. The aggregation can be inhibited when metal nanoparticles are deposited on the graphene surface. Metal nanoparticles introduced onto the surface of the graphene prevent the aggregation and provide good photoconductivity and catalytic properties of the graphene/metal nanocomposites [33,34]. The good conductivity, strong ultraviolet–visible absorption ability and catalytic activity of silver nanoparticles are the reason for their popularity in many fields, such as electronic devices, biomarkers and antibacterial agents [35]. Recently, the interest around graphene/metal nanoparticle composites has been growing, especially in the fields of catalysis, supercapacitors, energy storage, biosensors, chemical sensors, solar cells, membrane and hydrogen storage [36]. The importance of complexity in the design of the composites is a result of the requirement of obtaining graphene as individual sheets.

In this study, we prepared foils containing nanogold/graphene (ALG/Au/GOX) and nanosilver/graphene (ALG/Ag/GOX) in a sodium alginate matrix and characterized their morphology, enzymatic susceptibility, physicochemical and microbiological properties.

2. Materials and Methods

2.1. Materials

Research-grade chemical reagents were used to prepare the nanocomposites, i.e., sodium alginate (Sigma-Aldrich, Poznan, Poland), glycerine (Sigma-Aldrich, 99.5%)—as an excipient (plasticizer)—AgNO$_3$ (Sigma-Aldrich, Poznan, Poland, 99.99%), HAuCl$_4$·H$_2$O (Sigma-Aldrich, 99.9%), D-(+)-xylose (Sigma-Aldrich, 99%)—as a reducer—and deionized water.

For microbiological studies, the following media used were: Mannitol Salt Lab-Agar (named Chapman's medium) (BIOMAXIMA, Lublin, Poland) and TSA (BIOMAXIMA, Lublin, Poland). Standard strains of bacteria from the ATCC collection purchased from LGC Standards (Poland) were used in the study, i.e., *Staphylococcus capitis* (ATTC 146), *Staphylococcus equorum* (ATTC 43958), *Staphylococcus haemolyticus* (ATTC 29970), *Staphylococcus lentus* (ATTC 29070), *Staphylococcus succins* (ATTC 7003), *Staphylococcus vitulinus* (ATTC 51145), *Salmonella enteritidis* (ATTC 13076), *Escherichia coli* (ATTC 25922) and three strains of *Staphylococcus aureus* (ATTC 25923, ATTC 29213, ATTC 33591).

Hydrolysis was performed using alginate lyase EC 4.2.2.3 (Sigma-Aldrich). Alginate lyase catalyzes the degradation of alginate by a β-elimination reaction. It cleaves the (1→4) bond between β-D-mannuronate and either α-L-guluronate or β-D-mannuronate, generating oligosaccharides with 4-deoxy-α-L-erythro-hex-4-enuronosyl groups at their non-reducing ends and β-D-mannuronate at the reducing end. Depending on the composition of the substrate, the enzyme produces oligosaccharides ranging from two to four residues, with preference for shorter products [37].

2.2. Obtaining Graphene Oxide (GOX)

Graphene oxide (GOX) was synthesized by the modified Hummers method [38]. Aqueous suspensions containing 0.1% of GOX in distilled water were prepared and treated with ultrasounds.

2.3. ALG Sample Preparation

A 4% sodium alginate solution was prepared by gelatinizing 4 g of sodium alginate (Sigma-Aldrich, Poznan, Poland) with 96 g of deionized water in a magnetic stirrer (Heidolph MR3002, Schwabach, Germany) with a connected thermostat (50 °C). After completion of the gelatinizing process, 2 g of glycerine (99.5%, Sigma-Aldrich, Poznan, Poland) was added as a plasticizer. Once a homogeneous and clear mixture was obtained, it was transferred quantitatively (35 g) to a Petri dish (two repetitions).

The prepared plates were left in an oven for 24 h at 40 °C. After this time, the dried samples were taken out and stored in a desiccator containing a solution of saturated magnesium nitrate at 20 °C which ensures a relative humidity of 65%, until the physicochemical and microbiological analyses were performed.

2.4. ALG/Au/GOX Sample Preparation

A 4% sodium alginate solution (Alg) was prepared by gelatinizing 4 g of sodium alginate (Sigma-Aldrich, Poznan, Poland) with 96 g of deionized water in a magnetic stirrer (Heidolph MR3002, Schwabach, Germany) with a connected thermostat (50 °C). After completion of the gelatinizing process, 2 g of glycerine (99.5%, Sigma-Aldrich, Poznan, Poland) was added as plasticizer.

An amount of 2.5 mL of 0.1% graphene oxide solution (GOX) was added to 100 mL of 4% Alg and placed in a mechanical stirrer (Heidolph RZR2020, Schwabach, Germany) for stirring. An amount of 0.75 mL of 0.02% $HAuCl_4$ solution and 1.5 mL of 4% D-(+)-xylose were then added to the gel. The prepared mixture was placed in a water bath at 55 °C while stirring with a mechanical stirrer (Heidolph RZR2020, Schwabach, Germany). After this time, it was transferred to an ultrasonic bath (POLSONIC, Warsaw, Poland) for another 10 min. After the whole process was completed, the resulting bionanocomposite (4% ALG/Au/GOX) was transferred quantitatively (35.0 g) to a Petri dish (two repetitions).

The prepared plates were left in an oven for 24 h at 40 °C. After this time, the dried foil samples were taken out and stored in a desiccator containing a solution of saturated magnesium nitrate at 20 °C, which ensures a relative humidity of 65%, until the physicochemical and microbiological analyses were performed.

2.5. ALG/Ag/GOX Sample Preparation

A 4% sodium alginate solution (Alg) was prepared by gelatinizing 4 g of sodium alginate (Sigma-Aldrich, Poznan, Poland) with 96 g of deionized water in a magnetic stirrer (Heidolph MR3002, Schwabach, Germany) with a connected thermostat (50 °C). After completion of the gelatinizing process, 2 g of glycerine (99.5%, Sigma-Aldrich, Poznan, Poland) was added as plasticizer.

An amount of 2.5 mL of 0.1% graphene oxide solution (GOX) was added to 100 mL of 4% Alg and placed in a mechanical stirrer (Heidolph RZR2020, Schwabach, Germany) for stirring. The mixture was then placed in a water bath at 70 °C while stirring with a mechanical stirrer (Heidolph RZR2020, Schwabach, Germany). An amount of 0.3 mL of

0.1 M AgNO$_3$ and 1.5 mL of 4% D-(+)-xylose were successively added to the gel. The temperature was reduced to 55 °C and the mixture was stirred for another 10 min. After this time, the mixture was transferred to an ultrasonic bath (POLSONIC, Warsaw, Poland) for another 10 min. After the whole process was completed, the resulting bionanocomposite (4%ALG/Ag/GOX) was transferred quantitatively (35 g) to a Petri dish (two repetitions).

The prepared plates were left in an oven for 24 h at 40 °C. After this time, the dried film samples were taken out and stored in a desiccator containing a solution of magnesium nitrate, which ensures humidity of 65%, until the physicochemical and microbiological analyses were performed.

The resulting flexible and transparent films are shown in Figure 1.
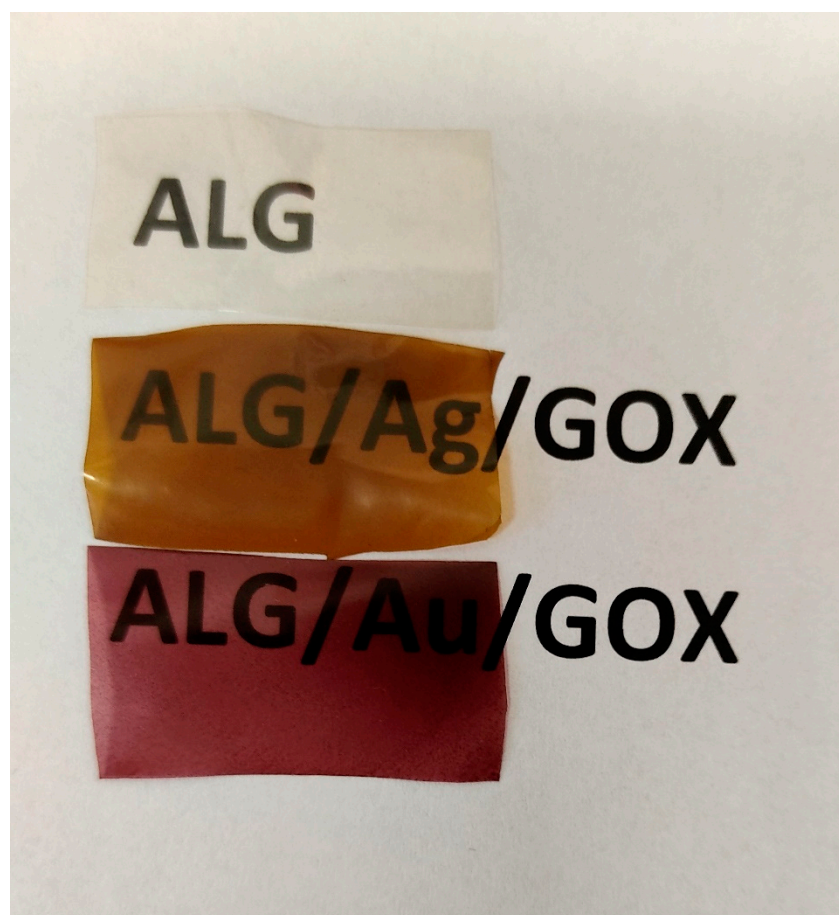
Figure 1. Obtained foils put on their printed names.

2.6. Scanning Electron Microscopy

The size and morphology of the as-prepared nanoparticles were recognized with a high resolution JEOL 7550 scanning electron microscope equipped with a Retractable Backscattered-Electron detector (RBEI).

2.7. FTIR-ATR Spectrophotometry

The FTIR–ATR spectra of the composites were recorded in the range of 4000–700 cm^{-1} using a MATTSON 3000 FT-IR (Madison, WI, USA) spectrophotometer. That instrument was equipped with a 30SPEC 30 Degree Reflectance adapter fitted with the MIRacle ATR accessory from PIKE Technologies Inc., Madison, WI, USA.

2.8. UV–Vis Absorption Spectrophotometry

The UV–vis absorption spectra of the composites were recorded using a Shimadzu 2101 scanning spectrophotometer in the range of 200–700 nm using 10 mL cells. The concentration of solution was 0.001 g/mL.

2.9. Wettability and Free Surface Energy Determination

Wettability on polysaccharide nanocomposites has always been a subject of considerable interest. Wettability experiments typically use the contact angle to characterize aqueous drops' wetting capacity on a solid surface and judge their suitability for different applications. Wettability affects ink receptivity, coating, absorbency, adhesion, and frictional properties. However, due in part to the rough, porous, and water-swellable nature of bio-polymer materials, poor fits between various theories and contact angle data have been observed. Therefore, the more sophisticated measurement of the surface free energy of solids is necessary for better material characterization.

In our research, we used the Drop Shape Analyzer Kruss DSA100M optical contact angle measuring instrument (Hamburg, Germany, Gmbh). The detailed methodology of the contact angle experiments, as well as the surface free energy analysis, were presented in our previous paper [20]. We used the Owens–Wendt method [39], which is generally accepted as the best for polymer evaluation. An exact and detailed introduction to the Owens–Wendt method was presented by Rudawska and co-workers [40]. All measurements were performed in the special environmental cell at constant temperature conditions ($22 \pm 0.3\,^\circ$C) and humidity. For each foil sample, more than three successive tests were carried out.

2.10. Differential Scanning Calorimetry

Differential scanning calorimetry (DSC) experiments were performed in a Mettler-Toledo 821e calorimeter equipped with an intracooler cooling system in 40 μL aluminum crucibles closed by a lid with a microhole under constant flow of argon or air (80 mL/min) within the temperature range of 25–500 $^\circ$C with a heating rate equal to 10 $^\circ$C/min.

2.11. Enzymatic Hydrolysis

Enzymatic hydrolysis of the films (0.1 g) was performed in a phosphate buffer with pH 7.0 (100 mL) using alginate lyase and 1.5 mL of enzyme solution (1 un/mL).

The mixtures were stirred (70 rpm) at $37 \pm 1\,^\circ$C for 5 h. During the reaction, at given time intervals, small amounts of the samples were removed, during which the enzyme was inactivated by 3,5-dinitrosalicylic acid (DNS) [41]. The concentration of oligosaccharides were determined according to Southgate (1991) [42] using a 2101PC, Shimadzu spectrophotometer set for k = 480–520 nm. D-Mannuronic acid sodium (Sigma-Aldrich) was the standard. Estimations were run in duplicate.

2.12. High Performance Size Exclusion Chromatography (HPSEC-MALLS-RI)

The samples of ALG and ALG/nanocomposite (100 mg) were dissolved in water (100 mL) and stirred afterwards for 12 h. Then, we used 0.8 mm cellulose acetate filters (Whatman, England) to filter the obtained solutions. The average molecular weight and radii of gyration were determined by a system consisting of a pump (Shimadzu 10AC, Tokyo, Japan), an injection valve (model 7021, Rheodyne, Palo Alto, CA, USA), a guard column TSK PWH (Tosoh Corporation, Tokyo, Japan), and two connected size exclusion columns TSKgel GMPWXL (300 × 7.8 mm, Tosoh Corporation, Tokyo, Japan) and TSKgel 2500 PWXL (300 × 7.8 mm, Tosoh Corporation, Tokyo, Japan). A multiangle laser light scattering detector (MALLS) operating in chromatographic mode using a He–Ne laser light source (630.0 nm) (Dawn-DSP-F, Wyatt Technology, Santa Barbara, CA, USA) and a differential refractive index detector (L-7490, Merck, Darmstadt, Germany) were connected to the columns. The columns were maintained at 30 $^\circ$C. The 0.2 and 0.1 μm cellulose acetate filters (Whatman, England) were used to filter the mobile phase (0.15 M NaNO$_3$ with 0.02% sodium azide). The flow

rate of the mobile phase and the sample injection volume were 0.4 mL/min and 500 μL, respectively. The Astra 4.73.04 software (Wyatt Technology, Santa Barbara, CA, USA) was used to calculate the average molecular weight (Mw) and radius of gyration (Rg) from the output voltage of refractive index (RI) and light scattering (LS) at 18 angles.

2.13. Bacteriostatic Activity Assay

The bacteriostatic properties of the obtained bionanocomposites were verified by microbiological tests using bacterial strains from the ATCC collection.

After isolating the pure cultures of bacteria, they were used to prepare suspensions in 0.85% saline solution (NaCl), whose optical density was 0.5 on the McFarland scale. The density was measured using a densitometer. Then, using a sterile swab stick, bacterial suspensions were inoculated onto previously prepared and solidified plates (Φ = 90 mm) with an equal volume (16 mL) of two Chapman microbiological media and TSA. Bacterial suspensions in the amount of 200 μL were inoculated with turf onto respective media. Four discs with a diameter of 0.5 cm of a given bionanocomposite were applied with tweezers onto the prepared culture. The plates were incubated for 48 h at 40 °C in an oxygen atmosphere. After this time, the plates were removed from the incubator and the zones of growth inhibition were measured.

3. Results and Discussion

In order to confirm the presence of silver and gold nanoparticles, to determine their size and to show the arrangement of graphene inside the bionanocomposite, analysis was performed using a scanning electron microscope. Graphene oxide–sodium alginate nanocomposites containing Ag and Au nanoparticles are shown in Figure 2.
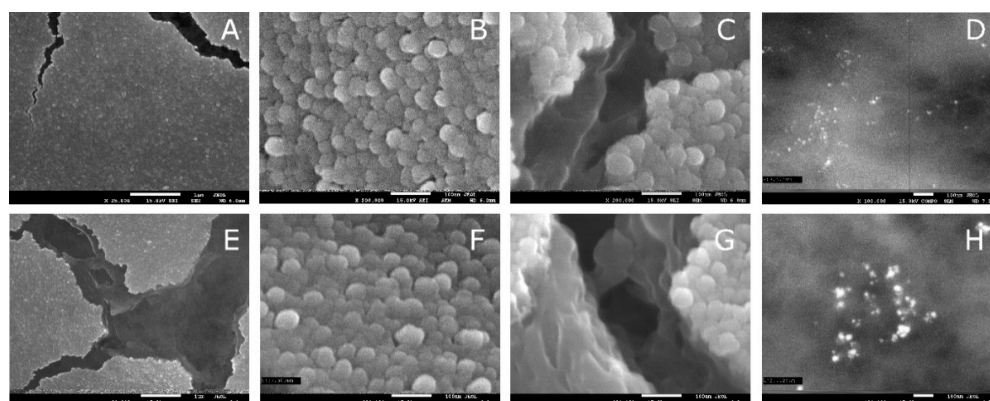
Figure 2. (**A**–**D**) SEM micrographs of ALG/Ag/GOX foils taken at different magnifications, 25,000×, 200,000×, 200,000×, 100,000×, respectively. (**E**–**H**) SEM micrographs of ALG/Au/GOX foils taken at different magnifications, 20,000×, 200,000×, 200,000×, 100,000×, respectively.

The surfaces of the obtained nanocomposites have a vesicular structure, which may be due to the fact that during nanoparticle generation, the alginate formed as nanocapsules with a size of about 20–50 nm (Figure 2B,F). During the measurement, due to the electron beam passing through the sample, numerous cracks were formed on the surface of the film (Figure 2C,G), allowing for the observation of the internal structure of the film. Figure 3 clearly shows that the internal structure of the film is porous; the resulting nanopores are most likely due to the presence of graphene oxide [43].
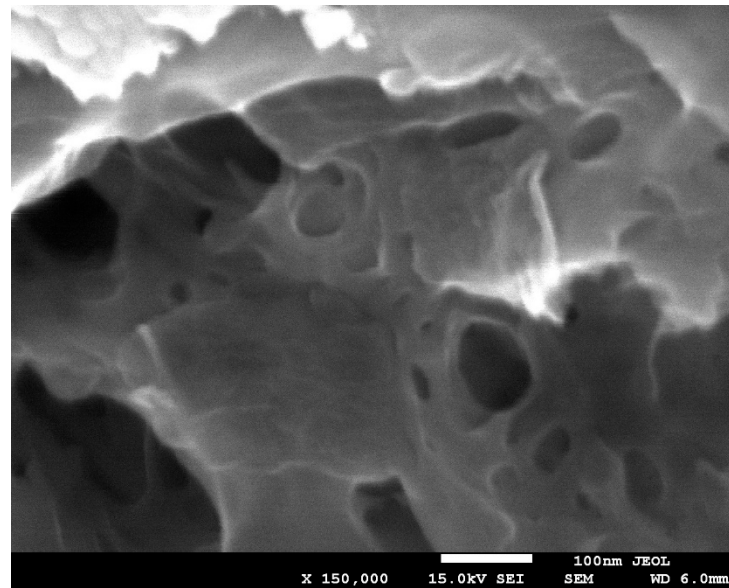
Figure 3. SEM micrograph taken at 150,000 magnification: ALG/Ag/GOX foil.

Using higher magnification in this method, we observe an alternating arrangement of graphene oxide sheets. By using secondary electron detection (in the COMPO system), the presence of nanogold and nanosilver in the whole structure of the obtained composites was proved (Figure 2D,H). The resulting silver nanostructures are characterized by different sizes; their sizes vary between 5–10 nm and 20–25 nm, while the average size of the obtained gold nanoparticles is about 10–20 nm. The obtained metal nanoparticles are in regular and spherical shapes.

Figure 4 shows the UV–vis absorption spectra of the control ALG sample and the ALG/Au/GOX and ALG/Ag/GOX nanocomposites, which show an absorption band at 540 nm for ALG/Au/GOX and between 380–550 nm for ALG/Ag/GOX. The results indicate the formation of Au and Ag nanoparticles [44]. The width of the peak band indicates that the formed nanoparticles are characterized by different sizes, which has already been confirmed by the scanning electron microscope (SEM) images.
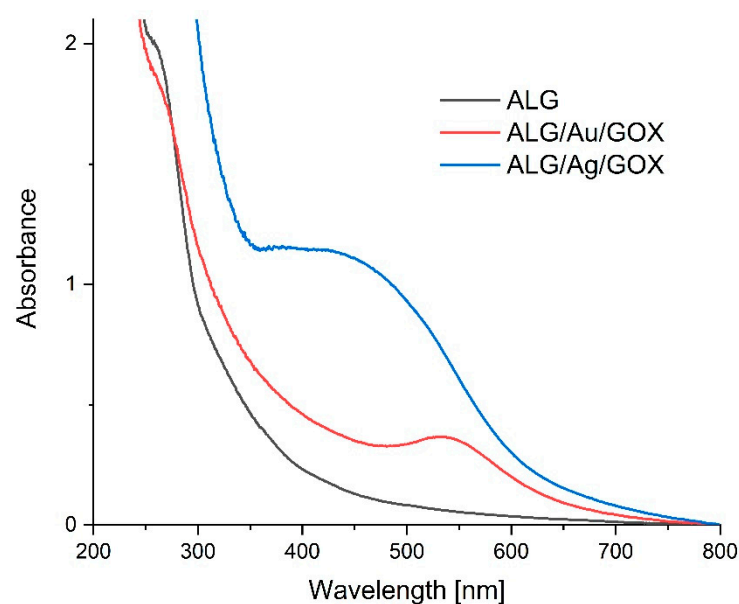
Figure 4. UV–vis spectra of ALG (black line), ALG/Au/GOX (red line) and ALG/Ag/GOX (blue line).

The FTIR absorption spectra of pure GOX and the obtained bionanocomposites are shown in Figure 5. GOX displayed characteristic FTIR peaks corresponding to its oxygen functionalities, including the C=O stretching vibration peak at 1731 cm^{-1}, the C-O (epoxy) stretching vibration peak at 1227 cm^{-1}, the C-O (alkoxy) stretching vibration peak at 1065 cm^{-1}, and the vibration and deformation peaks of O-H groups at 3412 cm^{-1} and 1627 cm^{-1}, respectively. The characteristic spectrum of the sodium alginate biopolymer is composed of a broad band centered at approximately 3219 cm^{-1} that arises from the stretching of hydroxyl groups, low intensity bands at about 2934 cm^{-1} attributed to –CH$_2$ groups, two peaks at 1597 cm^{-1} and 1404 cm^{-1} that come from the asymmetric and symmetric stretching modes, respectively, of carboxylate salt groups (-COONa), and a number of vibrations in the range 1100–1000 cm^{-1} assigned to the glycoside bonds in the polysaccharide (C-O-C stretching) [45]. The absence of significant changes in the shape of the obtained spectra indicates that the synthesis of nanometals did not cause structural changes in the alginate molecule. The decrease in the absorbance at 3219 cm^{-1}, 2934 cm^{-1}, 1597 cm^{-1} and 1401 cm^{-1} could be explained by different water content and various intermolecular interactions (e.g., hydrogen bonds) between polysaccharide molecules and GOX and indicate that there should be good miscibility between ALG and GOX [46]. The decrease in the absorbance could be explained by different water content and various intermolecular interactions between polysaccharide molecules and nanoparticles.
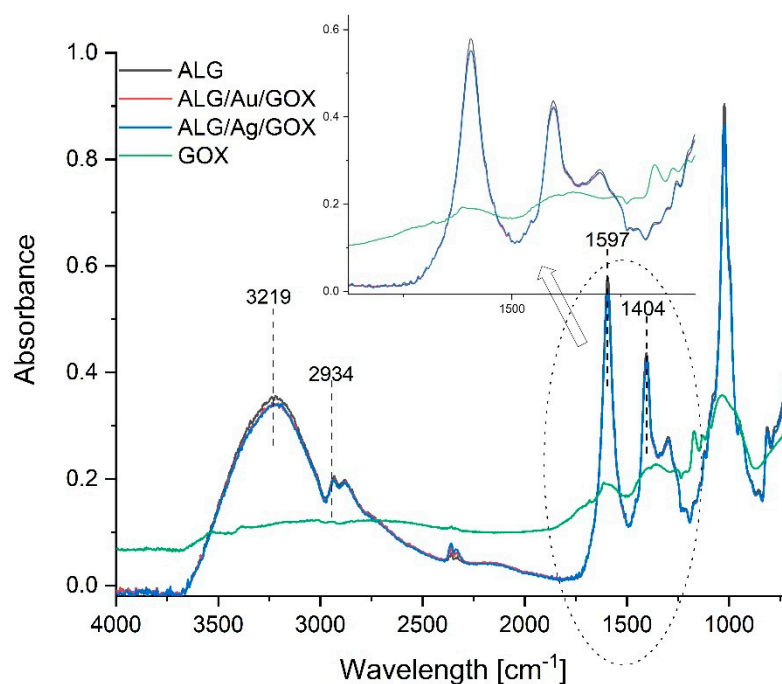

Figure 5. FTIR spectra of ALG (black line), ALG/Au/GOX (red line), ALG/Ag/GOX (blue line) and GOX (green line).

Size exclusion chromatography results are presented in Table 1. It shows an increase in the molecular weight in the samples containing nanoparticles. The highest increase was observed after the generation of Au nanoparticles. We could also notice an increase in the radii of gyration in both nanomaterial solutions compared to native ALG. This observation can be explained by interactions between sodium alginate, graphene oxide and nanometals.

The DSC charts presented in Figures 6 and 7 show that as a result of heating, all samples release water which is observed in the first endo peaks. The ALG/Au/GOX and ALG/Ag/GOX samples have peaks shifting towards higher temperatures (maximum above 100 °C) relative to the reference sample (ALG) which indicates a higher water binding enthalpy. These samples bind more water and to a stronger extent than the sample with sodium alginate alone. Water in the nanosilver sample is bound more strongly than

water in the nanogold sample. In contrast, the water content of the nanogold sample is slightly higher than that of the nanosilver sample. The strong endo effect at 195–196 °C for the ALG/Ag/GOX sample in air and argon indicates the rapid evaporation of water due to vesicle rupture. This indicates that the texture of this porous material is tight and has closed vesicles. The ALG/Au/GOX sample also shows a similar effect, but it is much smaller, which may indicate that the vesicles are much smaller due to the smaller size of the gold nanoparticles. The sample containing only sodium alginate does not have this endo peak. All samples are stable up to a temperature of about 200 °C.
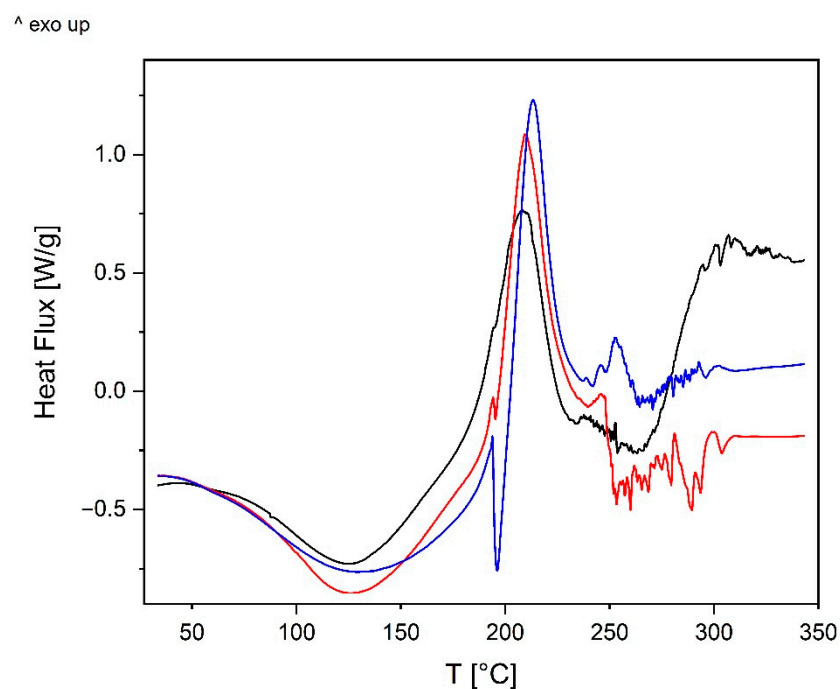
Figure 6. DSC chart in argon: ALG (black line), ALG/Ag/GOX (blue line), ALG/Au/GOX (red line).
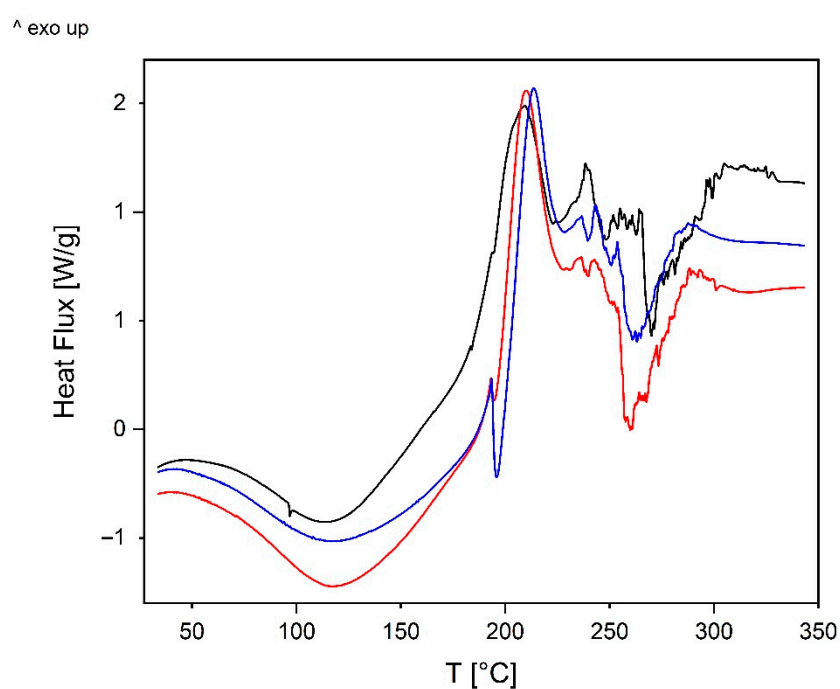
Figure 7. DSC chart in air: ALG (black line), ALG/Ag/GOX (blue line), ALG/Au/GOX (red line).

Table 1. The average molecular weight (Mw) and radius of gyration (Rg) of ALG, ALG/Au/GOX and ALG/Ag/GOX.

| Sample	Mw (Da)	Rg (nm)
ALG	1.565×10^5	43.9
ALG/Au/GOX	3.878×10^5	59.3
ALG/Ag/GOX	3.496×10^5	56.2

The exo peak in the range of 205–215 °C comes from sodium alginate. The system obtains stabilization and releases energy which may be related to crosslinking. Above 215 °C, there are thermal effects, characteristic of the caramelization and carbonization of polysaccharides.

The results of the wettability of the samples and the surface free energy are presented in Table 2. As can be seen, the wettability of the samples differs slightly after adding silver or gold nanoparticles. However, the difference between the samples is not that big. Only the ALG/Ag/GOX film shows slightly greater hydrophobic properties than the original reference ALG alginate film. The surface free energy analysis confirms the initial assumptions of the wettability research. In foil containing silver, the dispersion energy is lower than in foil without any additives (or in foil with gold). The obtained results also correlate with the DSC results.

The two-step hydrolysis reaction of materials by alginate lyase is a zero-order reaction, where v = k (curves depicting oligosaccharides vs. reaction time are linear (Figure 8)). The reaction rate constants of each step were determined by a graphical method (linear regression) [47]. The inverse value of the line slope coefficient equals the value of the reaction rate constant (Table 3).

Table 2. The wettability and surface free energy of studied foil samples: ALG, ALG/Au/GOX and ALG/Ag/GOX.

Sample	Contact Angle		Surface Free Energy		
	Water	Diiodomethane	Polar (mJ/m^2)	Dispersive (mJ/m^2)	Total Free Energy (mJ/m^2)
ALG	36.95	52.8	22.80	36.74	59.54
ALG/Au/GOX	39.8	56	21.30	35.98	57.28
ALG/Ag/GOX	46.95	56.15	22.34	30.10	52.44
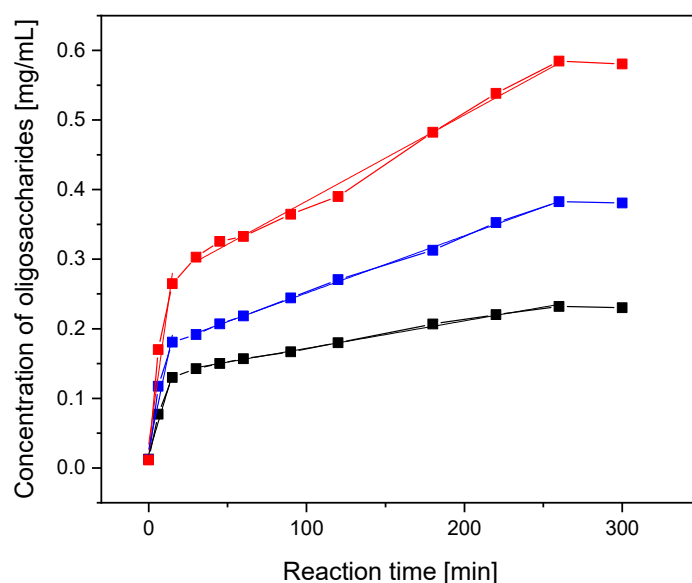
Figure 8. Graph showing the relationship between the reaction time and reducing sugar concentration of: ALG (black line), ALG/Ag/GOX (blue line), ALG/Au/GOX (red line).

Table 3. Values of rate constants (k) and hydrolysis yields (W).

| Sample	$k_1 \times 10^{-2}$ (mg·mL^{-1}·min^{-1})	$k_1 \times 10^{-4}$ (mg·mL^{-1}·min^{-1})	W (%)
ALG	0.8 ± 0.1	3.95 ± 0.09	58.0
ALG/Ag/GOX	1.1 ± 0.2	8.2 ± 0.1	38.1
ALG/Au/GOX	1.6 ± 0.2	12.4 ± 0.3	23.0

The reaction efficiency (Table 3) of hydrolysis was calculated using Equation (1):

$$W = (GD/GT) \cdot 100\% \tag{1}$$

where W denotes the reaction efficiency, GD is the amount of oligosaccharides received in the reaction, and GT is the theoretical amount of oligosaccharides resulting from the reaction equation.

The literature reports on the bactericidal and bacteriostatic effects of graphene [48], so for microbiological tests, another control sample—ALG/GOX—was prepared analogously to the previous ones, but without generating nanoparticles.

The inhibition of the growth of *Escherichia coli* occurs in all composites tested (Figure 9). In the case of ALG, this is the smallest inhibition at 13 mm. The ALG/GOX composite (14 mm) inhibits *E. coli* growth at a similar level as the ALG/Au/GOX nanocomposite (16 mm). The highest inhibition of bacterial growth is observed under the influence of ALG/Ag/GOX (27 mm).
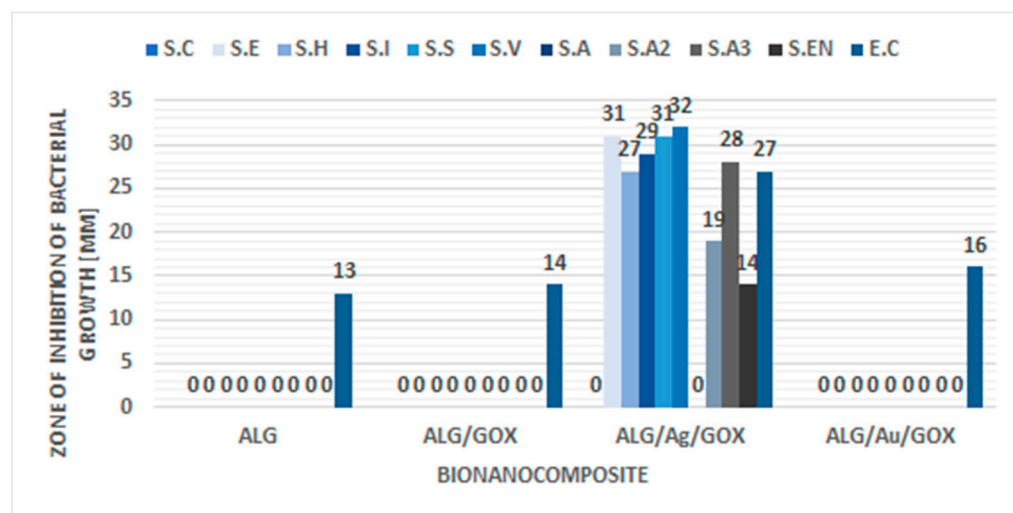
Figure 9. Growth inhibition zones for bacteria *Staphylococcus capitis* (S.C), *Staphylococcus equorum* (S.E), *Staphylococcus haemolyticus* (S.H), *Staphylococcus lentus* (S.L), *Staphylococcus succins* (S.S), *Staphylococcus vitulinus* (S.V), *Staphylococcus aureus 1* (S.A), *Staphylococcus aureus 2* (S.A2), *Staphylococcus aureus 3* (S.A3), *Salmonella enteritidis* (S.EN), *Escherichia coli* (E.C).

For the other bacteria analyzed, no zones of growth inhibition were demonstrated under the influence of ALG, ALG/GOX and ALG/Au/GOX.

It was demonstrated that nanosilver has a much greater antimicrobial effect than ionic silver. One of the pathways of antimicrobial action of nanosilver is its ability to release silver ions, which can interact with bacterial cell walls, their plasma membranes, proteins, ribosomes or bacterial DNA [49–53]. The bacterial cell wall consists of a peptidoglycan, which contains receptors and enzymes responsible for bacterial cell respiration. The binding of thiol proteins with silver causes their abnormal folding and denaturation. This results in the inactivation of key enzyme proteins including respiratory chain proteins. This results in cell death due to oxidative stress [54–56]. Another pathway of action of

nanosilver is the accumulation of particles in battery sheaths. This leads to the formation of pores with irregular edges, which disrupts the ion transport process, causes membrane de-energization and, consequently, cell death. Nucleic acids of bacterial cells contain phosphorus and sulfur, which has affinity for nanosilver, which is a chemically weak acid. The binding of nanoparticles to DNA results in the inhibition of DNA replication, or its complete destruction. As a result of the reaction of nanosilver with the protein S6 from the 30S ribosomal subunit, the translation process may be disturbed. This results from the inhibition of membrane protein biosynthesis and heat shock, and the cells are deprived of protection against oxidative stress damage [57].

In all samples, a zone of microbial growth inhibition of similar size was observed only for *E. coli*. This inhibition may be due to the formation of an alkaline environment, for which bacteria in the genus *Staphylococcus*, in which no zone of growth inhibition is observed, have a higher tolerance. The absence of growth inhibition zones in the case of the alginate–graphene composite may be due to the presence of polymer. The polymer chains surrounding the graphene sheets round off their sharp edges. The mechanism of graphene's bactericidal action is directly related to the sharp edges of the sheets, which cause the mechanical destruction of cell membranes. Thus, smoothing the edges leads to the deactivation of the antimicrobial action [58]. The zone of growth inhibition for *Escherichia coli* when exposed to nanogold may also result from the impairment of proteins, lipids and nucleic acids present in bacterial cell membranes [59,60]. The absence of inhibition zones for microbial growth after 48 h of incubation in the case of nanogold is not a result that excludes its antimicrobial activity. The antimicrobial properties of nanometals are influenced by their shape, size or surface-to-volume ratio. It also depends on the diffusion mechanisms in the growth media. One of the described ways of the influence of nanometals on microorganisms is the ion release—the lower activity of nanogold can be caused by the slower ion release compared to nanosilver [61–63]. It seems reasonable to continue microbiological studies over longer incubation periods or increased nanogold concentrations [60].

4. Conclusions

The results of our study show that the synthesis of silver and gold nanoparticles can be successfully performed with environmentally friendly methods, using sodium alginate as a stabilizing template. Gold nanocrystals provided in sodium alginate matrices are uniform in size and shape and exhibited the lowest polydispersity. In addition, SEM evidenced a uniform distribution of GOX sheets within ALG matrix. FT-IR and size exclusion chromatography results suggested that GOX sheets, containing abundant functional groups on the surface, form an interaction with the sodium alginate matrix. The incorporation of GOX sheets within the ALG matrix has a beneficial effect on the thermal stability of nanocomposite films. Nanocomposites exhibited an increased enzymatic hydrolysis rate constant—the obtained films underwent the hydrolysis reaction faster and hydrolyzed to a greater extent than the alginate itself. Prepared composite containing silver nanocomposites exhibited slightly greater hydrophobic properties, lower dispersion and surface free energy, and bacteriostatic activity against tested microorganisms. The obtained foils, due to the described properties caused by the presence of nanoparticles, are expected to be successfully used in various branches of industry (for example in food packaging, drug delivery, tissue engineering). The higher susceptibility to hydrolysis suggests that their biodegradation would occur faster, and the foils would cause less harm to the environment.

Author Contributions: Conceptualization, G.K. and K.K.; methodology, G.K., K.K., A.K.-M., M.K., N.N., W.G.; software, K.K. and A.K.-M.; validation, G.K., J.G. and M.K.; formal analysis, G.K., K.K., N.N., W.G., A.K.-M. and M.K.; investigation, G.K. and K.K.; data curation, K.K., A.K.-M. and M.K.; writing—original draft preparation, G.K., K.K., N.N. and W.G.; writing—review and editing, G.K. and K.K.; visualization, K.K.; supervision, G.K. All authors have read and agreed to the published version of the manuscript.

Institutional Review Board Statement: Not applicable.

Informed Consent Statement: Not applicable.

Data Availability Statement: Not applicable.

Conflicts of Interest: The authors declare no conflict of interest.

References

1. Cumpstey, I. Chemical Modification of Polysaccharides. *Int. Sch. Res. Not.* **2013**, *2013*, 27. [CrossRef]
2. Li, S.; Xiong, Q.; Lai, X.; Li, X.; Wan, M.; Zhang, J.; Yan, Y.; Cao, M.; Lu, L.; Guan, J.; et al. Molecular Modification of Polysaccharides and Resulting Bioactivities. *Compr. Rev. Food Sci. Food Saf.* **2016**, *15*, 237–250. [CrossRef] [PubMed]
3. Gamal-Eldeen, A.M.; Ahmed, E.F.; Abo-Zeid, M.A. In vitro cancer chemopreventive properties of polysaccharide extract from the brown alga, Sargassum latifolium. *Food Chem. Toxicol.* **2009**, *47*, 1378–1384. [CrossRef] [PubMed]
4. Tian, Y.; Zeng, H.; Xu, Z.; Zheng, B.; Lin, Y.; Gan, C.; Lo, Y.M. Ultrasonic-assisted extraction and antioxidant activity of polysaccharides recovered from white button mushroom (*Agaricus bisporus*). *Carbohydr. Polym.* **2012**, *88*, 522–529. [CrossRef]
5. Li, S.; Shah, N.P. Antioxidant and antibacterial activities of sulphated polysaccharides from Pleurotus eryngii and Streptococcus thermophilus ASCC 1275. *Food Chem.* **2014**, *165*, 262–270. [CrossRef]
6. Martí, M.; Frígols, B.; Salesa, B.; Serrano-Aroca, Á. Calcium alginate/graphene oxide films: Reinforced composites able to prevent Staphylococcus aureus and methicillin-resistant Staphylococcus epidermidis infections with no cytotoxicity for human keratinocyte HaCaT cells. *Eur. Polym. J.* **2019**, *110*, 14–21. [CrossRef]
7. Senturk Parreidt, T.; Müller, K.; Schmid, M. Alginate-Based Edible Films and Coatings for Food Packaging Applications. *Foods* **2018**, *7*, 170. [CrossRef]
8. Batista, P.S.P.; de Morais, A.M.M.B.; Pintado, M.M.E.; de Morais, R.M.S.C. *Alginate: Pharmaceutical and Medical Applications*; Springer: Cham, Switzerland, 2019; pp. 649–691.
9. Salesa, B.; Llorens-Gámez, M.; Serrano-Aroca, Á. Study of 1D and 2D Carbon Nanomaterial in Alginate Films. *Nanomaterials* **2020**, *10*, 206. [CrossRef] [PubMed]
10. Darder, M.; Aranda, P.; Ruiz-Hitzky, E. Bionanocomposites: A New Concept of Ecological, Bioinspired, and Functional Hybrid Materials. *Adv. Mater.* **2007**, *19*, 1309–1319. [CrossRef]
11. Dias, A.M.G.C.; Hussain, A.; Marcos, A.S.; Roque, A.C.A. A biotechnological perspective on the application of iron oxide magnetic colloids modified with polysaccharides. *Biotechnol. Adv.* **2011**, *29*, 142–155. [CrossRef]
12. Hanemann, T.; Szabó, D.V. Polymer-Nanoparticle Composites: From Synthesis to Modern Applications. *Materials* **2010**, *3*, 3468–3517. [CrossRef]
13. Emam, H.E.; Ahmed, H.B. Polysaccharides templates for assembly of nanosilver. *Carbohydr. Polym.* **2016**, *135*, 300–307. [CrossRef]
14. Martínez, A.M.; Benito, M.; Pérez, E.; María Teijón, J.; Dolores Blanco, M. The Role of Anionic Polysaccharides in the Preparation of Nanomedicines with Anticancer Applications. *Curr. Pharm. Des.* **2016**, *22*, 3364–3379. [CrossRef]
15. Yang, C.H.; Wang, L.S.; Chen, S.Y.; Huang, M.C.; Li, Y.H.; Lin, Y.C.; Chen, P.F.; Shaw, J.F.; Huang, K.S. Microfluidic assisted synthesis of silver nanoparticle–chitosan composite microparticles for antibacterial applications. *Int. J. Pharm.* **2016**, *510*, 493–500. [CrossRef]
16. Kemp, M.M.; Kumar, A.; Clement, D.; Ajayan, P.; Mousa, S.; Linhardt, R.J. Hyaluronan- and heparin-reduced silver nanoparticles with antimicrobial properties. *Nanomedicine* **2009**, *4*, 421–429. [CrossRef] [PubMed]
17. Jamróz, E.; Khachatryan, G.; Kopel, P.; Juszczak, L.; Kawecka, A.; Krzyściak, P.; Kucharek, M.; Bębenek, Z.; Zimowska, M. Furcellaran nanocomposite films: The effect of nanofillers on the structural, thermal, mechanical and antimicrobial properties of biopolymer films. *Carbohydr. Polym.* **2020**, *240*, 116244. [CrossRef]
18. Khachatryan, G.; Khachatryan, K.; Stobinski, L.; Tomasik, P.; Fiedorowicz, M.; Lin, H.M. CdS and ZnS quantum dots embedded in hyaluronic acid films. *J. Alloys Compd.* **2009**, *481*, 402–406. [CrossRef]
19. Khachatryan, G.; Khachatryan, K.; Grzyb, J.; Fiedorowicz, M. Formation and properties of hyaluronan/nano Ag and hyaluronan-lecithin/nano Ag films. *Carbohydr. Polym.* **2016**, *151*, 452–457. [CrossRef]
20. Khachatryan, G.; Khachatryan, K.; Krystyjan, M.; Krzan, M.; Khachatryan, L. Functional properties of composites containing silver nanoparticles embedded in hyaluronan and hyaluronan-lecithin matrix. *Int. J. Biol. Macromol.* **2020**, *149*, 417–423. [CrossRef]
21. Maftoonazad, N.; Ramaswamy, H.S.; Marcotte, M. Shelf-life extension of peaches through sodium alginate and methyl cellulose edible coatings. *Int. J. Food Sci. Technol.* **2008**, *43*, 951–957. [CrossRef]
22. Yang, L.; Paulson, A.T. Mechanical and water vapour barrier properties of edible gellan films. *Food Res. Int.* **2000**, *33*, 563–570. [CrossRef]
23. Coleman, J.N.; Khan, U.; Blau, W.J.; Gun'ko, Y.K. Small but strong: A review of the mechanical properties of carbon nanotube-polymer composites. *Carbon N. Y.* **2006**, *44*, 1624–1652. [CrossRef]
24. Han, Z.; Fina, A. Thermal conductivity of carbon nanotubes and their polymer nanocomposites: A review. *Prog. Polym. Sci.* **2011**, *36*, 914–944. [CrossRef]
25. Rodríguez-González, C.; Martínez-Hernández, A.L.; Castanõ, V.M.; Kharissova, O.V.; Ruoff, R.S.; Velasco-Santos, C. Polysaccharide nanocomposites reinforced with graphene oxide and keratin-grafted graphene oxide. *Ind. Eng. Chem. Res.* **2012**, *51*, 3619–3629. [CrossRef]

26. Wang, J.; Jin, X.; Li, C.; Wang, W.; Wu, H.; Guo, S. Graphene and graphene derivatives toughening polymers: Toward high toughness and strength. *Chem. Eng. J.* **2019**, *370*, 831–854. [CrossRef]

27. Qi, Y.; Yang, M.; Xu, W.; He, S.; Men, Y. Natural polysaccharides-modified graphene oxide for adsorption of organic dyes from aqueous solutions. *J. Colloid Interface Sci.* **2017**, *486*, 84–96. [CrossRef]

28. Akhavan, O.; Ghaderi, E.; Aghayee, S.; Fereydooni, Y.; Talebi, A. The use of a glucose-reduced graphene oxide suspension for photothermal cancer therapy. *J. Mater. Chem.* **2012**, *22*, 13773–13781. [CrossRef]

29. Song, E.; Han, W.; Li, C.; Cheng, D.; Li, L.; Liu, L.; Zhu, G.; Song, Y.; Tan, W. Hyaluronic acid-decorated graphene oxide nanohybrids as nanocarriers for targeted and pH-responsive anticancer drug delivery. *ACS Appl. Mater. Interfaces* **2014**, *6*, 11882–11890. [CrossRef] [PubMed]

30. Kumar, P.; Huo, P.; Zhang, R.; Liu, B. Antibacterial Properties of Graphene-Based Nanomaterials. *Nanomaterials* **2019**, *9*, 737. [CrossRef]

31. Li, J.; Wang, G.; Zhu, H.; Zhang, M.; Zheng, X.; Di, Z.; Liu, X.; Wang, X. Antibacterial activity of large-area monolayer graphene film manipulated by charge transfer. *Sci. Rep.* **2014**, *4*, 1–8. [CrossRef] [PubMed]

32. Narayanan, K.B.; Park, G.T.; Han, S.S. Antibacterial properties of starch-reduced graphene oxide–polyiodide nanocomposite. *Food Chem.* **2021**, *342*, 128385. [CrossRef] [PubMed]

33. Xu, C.; Wang, X.; Zhu, J. Graphene—Metal particle nanocomposites. *J. Phys. Chem. C* **2008**, *112*, 19841–19845. [CrossRef]

34. Wang, W.; Wang, W.; Chen, X.; Wu, Y.; Dong, L. Synthesis and characterization of Ag/graphene nano-composite. *Xiyou Jinshu Cailiao Yu Gongcheng/Rare Met. Mater. Eng.* **2015**, *44*, 2138–2142. [CrossRef]

35. Shen, J.; Shi, M.; Li, N.; Yan, B.; Ma, H.; Hu, Y.; Ye, M. Facile Synthesis and Application of Ag-Chemically Converted Graphene Nanocomposite. *Nano Res.* **2010**, *3*, 339–349. [CrossRef]

36. Lawal, A.T. Graphene-based nano composites and their applications. A review. *Biosens. Bioelectron.* **2019**, *141*, 111384. [CrossRef]

37. EC 4.2.2.3. Available online: https://www.qmul.ac.uk/sbcs/iubmb/enzyme/EC4/2/2/3.html (accessed on 12 March 2021).

38. Stobinski, L.; Lesiak, B.; Malolepszy, A.; Mazurkiewicz, M.; Mierzwa, B.; Zemek, J.; Jiricek, P.; Bieloshapka, I. Graphene oxide and reduced graphene oxide studied by the XRD, TEM and electron spectroscopy methods. *J. Electron. Spectros. Relat. Phenom.* **2014**, *195*, 145–154. [CrossRef]

39. Owens, D.K.; Wendt, R.C. Estimation of the surface free energy of polymers. *J. Appl. Polym. Sci.* **1969**. [CrossRef]

40. Rudawska, A.; Jacniacka, E. Analysis for determining surface free energy uncertainty by the Owen-Wendt method. *Int. J. Adhes. Adhes.* **2009**. [CrossRef]

41. Fiedorowicz, M.; Khachatryan, G.; Konieczna-Molenda, A.; Tomasik, P. Formation of cyclodextrins with cyclodextrin glucosyltransferase stimulated with polarized light. *Biotechnol. Prog.* **2009**, *25*, 147–150. [CrossRef]

42. Southgate, D.A.T. *Determination of Food Carbohydrates*, 2nd ed.; Elsevier: Amsterdam, The Netherlands, 1991; ISBN 1-85166-652-4.

43. Tang, M.; Jiang, J.; Lv, Q.; Yang, B.; Zheng, M.; Gao, X.; Han, J.; Zhang, Y.; Yang, Y. Denitrification performance of Pseudomonas fluorescens Z03 immobilized by graphene oxide-modified polyvinyl-alcohol and sodium alginate gel beads at low temperature. *R. Soc. Open Sci.* **2020**, *7*. [CrossRef]

44. Khachatryan, K.; Khachatryan, G.; Fiedorowicz, M.; Para, A.; Tomasik, P. Formation of nanometal particles in the dialdehyde starch matrix. *Carbohydr. Polym.* **2013**, *98*, 568–573. [CrossRef]

45. Nalini, T.; Basha, S.K.; Mohamed Sadiq, A.M.; Kumari, V.S.; Kaviyarasu, K. Development and characterization of alginate/chitosan nanoparticulate system for hydrophobic drug encapsulation. *J. Drug Deliv. Sci. Technol.* **2019**, *52*, 65–72. [CrossRef]

46. Zheng, H.; Yang, J.; Han, S. The synthesis and characteristics of sodium alginate/graphene oxide composite films crosslinked with multivalent cations. *J. Appl. Polym. Sci.* **2016**, *133*. [CrossRef]

47. Konieczna-Molenda, A.; Kochanowski, A.; Walaszek, A.; Bortel, E.; Tomasik, P. Immobilization of α-amylase on poly(vinylamine) and poly(vinylformamide) supports and its performance. *Chem. Eng. J.* **2009**, *146*, 515–519. [CrossRef]

48. Pandit, S.; Cao, Z.; Mokkapati, V.R.S.S.; Celauro, E.; Yurgens, A.; Lovmar, M.; Westerlund, F.; Sun, J.; Mijakovic, I. Vertically Aligned Graphene Coating is Bactericidal and Prevents the Formation of Bacterial Biofilms. *Adv. Mater. Interfaces* **2018**, *5*, 1701331. [CrossRef]

49. Chaloupka, K.; Malam, Y.; Seifalian, A.M. Nanosilver as a new generation of nanoproduct in biomedical applications. *Trends Biotechnol.* **2010**, *28*, 580–588. [CrossRef]

50. Woo, K.J.; Hye, C.K.; Ki, W.K.; Shin, S.; So, H.K.; Yong, H.P. Antibacterial activity and mechanism of action of the silver ion in Staphylococcus aureus and Escherichia coli. *Appl. Environ. Microbiol.* **2008**, *74*, 2171–2178. [CrossRef]

51. Yamanaka, M.; Hara, K.; Kudo, J. Bactericidal actions of a silver ion solution on Escherichia coli, studied by energy-filtering transmission electron microscopy and proteomic analysis. *Appl. Environ. Microbiol.* **2005**, *71*, 7589–7593. [CrossRef]

52. Shrivastava, S.; Bera, T.; Roy, A.; Singh, G.; Ramachandrarao, P.; Dash, D. Characterization of enhanced antibacterial effects of novel silver nanoparticles. *Nanotechnology* **2007**, *18*, 225103. [CrossRef]

53. Yang, W.; Shen, C.; Ji, Q.; An, H.; Wang, J.; Liu, Q.; Zhang, Z. Food storage material silver nanoparticles interfere with DNA replication fidelity and bind with DNA. *Nanotechnology* **2009**, *20*, 085102. [CrossRef] [PubMed]

54. Kim, J.S.; Kuk, E.; Yu, K.N.; Kim, J.H.; Park, S.J.; Lee, H.J.; Kim, S.H.; Park, Y.K.; Park, Y.H.; Hwang, C.Y.; et al. Antimicrobial effects of silver nanoparticles. *Nanomed. Nanotechnol. Biol. Med.* **2007**, *3*, 95–101. [CrossRef]

55. Cho, K.H.; Park, J.E.; Osaka, T.; Park, S.G. The study of antimicrobial activity and preservative effects of nanosilver ingredient. *Electrochim. Acta* **2005**, *51*, 956–960. [CrossRef]

56. Spacciapoli, P.; Buxton, D.; Rothstein, D.; Friden, P. Antimicrobial activity of silver nitrate against periodontal pathogens. *J. Periodontal Res.* **2001**, *36*, 108–113. [CrossRef] [PubMed]

57. Kurantowicz, N.; Sawosz, E.; Jaworski, S.; Kutwin, M.; Strojny, B.; Wierzbicki, M.; Szeliga, J.; Hotowy, A.; Lipińska, L.; Koziński, R.; et al. Interaction of graphene family materials with Listeria monocytogenes and Salmonella enterica. *Nanoscale Res. Lett.* **2015**, *10*, 1–12. [CrossRef]

58. Bykkam, S.; Narsingam, S.; Ahmadipour, M.; Dayakar, T.; Venkateswara Rao, K.; Shilpa Chakra, C.; Kalakotla, S. Few layered graphene Sheet decorated by ZnO Nanoparticles for anti-bacterial application. *Superlattices Microstruct.* **2015**, *83*, 776–784. [CrossRef]

59. Tao, C. Antimicrobial activity and toxicity of gold nanoparticles: Research progress, challenges and prospects. *Lett. Appl. Microbiol.* **2018**, *67*, 537–543. [CrossRef] [PubMed]

60. Su, C.; Huang, K.; Li, H.H.; Lu, Y.G.; Zheng, D.L. Antibacterial Properties of Functionalized Gold Nanoparticles and Their Application in Oral Biology. *J. Nanomater.* **2020**, *2020*. [CrossRef]

61. Morales-Avila, E.; Ferro-Flores, G.; Ocampo-García, B.E.; López-Téllez, G.; López-Ortega, J.; Rogel-Ayala, D.G.; Sánchez-Padilla, D. Antibacterial Efficacy of Gold and Silver Nanoparticles Functionalized with the Ubiquicidin (29–41) Antimicrobial Peptide. *J. Nanomater.* **2017**, *2017*, 1–10. [CrossRef]

62. Zhou, Y.; Kong, Y.; Kundu, S.; Cirillo, J.D.; Liang, H. Antibacterial activities of gold and silver nanoparticles against Escherichia coli and bacillus Calmette-Guérin. *J. Nanobiotechnol.* **2012**, *10*, 19. [CrossRef] [PubMed]

63. Johnston, J.H.; Nilsson, T. Nanogold and nanosilver composites with lignin-containing cellulose fibres. *J. Mater. Sci.* **2012**, *47*, 1103–1112. [CrossRef]